Version of Record: https://www.sciencedirect.com/science/article/pii/S0749641919307065
Manuscript_99a17ceabfe31facd22d169e3861130c

A Multi-physics Constitutive Model to Predict Quasi-static Behaviour: Hydrolytic Aging in Thin Cross-linked Polymers

Amir Bahrololoumi[a,c], Vahid Morovati[a,d], Emad A. Poshtan[b,e], Roozbeh Dargazany[1 a,f]

[a] *Department of Civil and Environmental Engineering, Michigan State University*
[b] *Robert Bosch Company, Reutlingen, Germany*
[c] *bahrolol@msu.edu*
[d] *morovati@msu.edu*
[e] *Emad.Poshtan@de.bosch.com*
[f] *roozbeh@msu.edu*

Abstract

The effect of hydrolytic aging on mechanical quasi-static responses of rubber-like materials, in particular, the idealized Mullins effect and permanent set have been modeled. The effect of Hydrolytic damage on the mechanical integrity of the polymer matrix is modeled as the direct competition of two micro-structural phenomena (i) chain scission and (ii) reduction of cross-links. Both phenomena and their correlation were modeled and thus, the strain energy of the polymer matrix is written with respect to three independent mechanisms; i) the shrinking original matrix that has not been attacked by water, ii) conversion of the first network to a new network due to the reduction of the crosslinks, and iii) energy loss from network degradation due to water attacks to polymer active agents. The proposed model satisfies the Clausius-Duhem inequality and is thus physically feasible. The model is validated with respect to sets of our experimental data and other sets available in the literature. The proposed model is based on the assumption of homogeneous diffusion and mainly relevant for thin samples. In view of its accuracy, interpret-ability and deep insight it provides into the nature of damage accumulation, the model is a good choice for further implementation in FE applications.

1. Introduction

In view of the high resistance to abrasion, corrosion and chemical degradation, elastomers are widely used in many sensitive applications to transfer load in high deformation regime or to dissipate kinetic energy in high frequency. In many industrial applications, it is necessary to provide a realistic approximation of the nominal service life of a sample subjected to specific loading profile. In many cases, elastomers are expected to sustain millions of load cycles or sustain extreme environmental loads for years, if not decades. However, environmental factors along with the mechanical loads will contribute to chemo-physical damages that will eventually lead to material failure [1]. Understanding the relation between chemical damages and decay in mechanical performance is critical for prediction of elastomers failure in extreme applications, such as offshore platforms. Such decay can be formed due to an individual or combined effects of different degradation processes [2]. Those mechanisms can be categorized into those with the major impacts such as thermo-oxidation [3, 4], hygro-thermal [5], hydrolysis [6, 7], deformation-induced aging [8, 9, 10] , and those with the less severe impact such as chemical corrosion [11], and ozone cracking [12]. While each of those mechanisms can significantly reduce the life of an elastomeric material in certain condition, the latter group are not as prevalent in nature as those of the first group are. The aging process can be formed due to an individual or combined effects of different degradation processes such as thermos-oxidation, photo-oxidation, and hydrolysis [13]. While predicting the individual contribution of those mechanisms have been the center of attention in the last few years, there is still a long way to go in modeling the damage accumulation in materials exposed to multiple damages simultaneously. To this end, reliable lifetime estimation of products made by cross-linked polymers can be extremely challenging, especially for the products that are exposed to multiple damages.

[1] Corresponding author.

Elastomeric systems are used in a variety of applications ranging from tires to adhesives, sealants, and thin films [14]. In view of their excellent properties, e.g. abrasion resistance and durability, elastomeric components can be reliably designed to be subjected to a high number of cyclic loading in harsh environments. However, their reliability considerably decreases over time due to the so-called aging process. The aging process, often described by a gradual decay of the mechanical performance, is a menace to the polymeric components such as joints, adhesives, sealant and fillers that are used in different components in multiple applications.

In the last 15 years, our predicative abilities has been significantly improved, and many theories were developed to describe different aging mechanisms, most of which were focused on thermo-oxidative aging. To this end, Loeffel and Anand [15] investigated a multi-physics model for the thermal oxidation aging of coatings in severe operating conditions. Some approaches described the thermo-oxidative aging of a polymer matrix with respect to the chemical reactions, diffusion and mechanical coupling [16, 17, 18], and some described it using the mechanism of curing [19, 20] . In all the aforementioned studies, the damage has been micro-mechanically modeled by a coupled approach to link chemical/physical aging to the thermo-mechanical state of the network [21, 22, 23].

The effect of time on constitutive behaviour of elastomers is often described by visco-elastic behavior, which is more of the short term effects of time [24, 25, 26]. Visco-elastic properties has been studies extensively both theoretically [27, 28] and experimentally [29]. Ayoub et al. [30] proposed a constitutive model using a Zener-type framework. Their model predicts the behavior by integrating the physics of polymer chains and their alteration under cyclic loading. Furthermore, Khan et al. [31] proposed a phenomenological model to characterize the thermo-mechanical behavior of visco-elastic polymers.

Here, we mainly focus on Quasi-static behaviour of samples submerged in water for a long time (hydrolytic aging) [32], e.g. those used in off-shore plants, biological systems or within the cooling systems [33]. At this stage, the model cannot take into account the effects of loading frequency as well as visco-elastic effects. In such applications, the predictive models can prevent catastrophic failure of the systems due to aging of components. To this end, a model for the Hydrolytic aging and its effect on the mechanical properties of rubber-like material can be subject of broader interest to our community. Hydrolytic aging can be described in two categories: physical or chemical [34]. Physical aging has no effect on the chemical structure and is a result of the movement of polymer chains. Chemical aging, on the other hand, is an irreversible process that changes the morphology of the matrix and directly affects the mechanical performance of the sample and probability of premature failure.

Hydroletic aging has been mostly studied through experimental studies. So far, only a few phenomenological models, and no micro-mechanical model, are available which can successfully take into account the effect of hydrolytic aging on behavior of elastomeric materials. Vieira et al. [35] proposed a model for hydrolytic aging of PLA-PCL fibers used in surgeries, and Breche et al. [36] who used a non-linear viscoelastic model to predict the response of biodegradable materials throughout hydrolytic aging. From experimental side, several studies were conducted to explore the relation between hydrolytic aging and loss of mechanical performance in different materials, such as poly-ester urethane [37], and thermoplastic polyurethanes [38]. On another approach, many studies were focused on describing the correlation between aging and changes of the matrix morphology, such as molecular weight [39], cross-link density [40] and formation/detachment of cross- links [41].

In this work, a new micro-mechanical model is developed to predict the non-linear behavior of rubber-like materials such as the Mullins effect and Permanent set during hydrolytic aging. "Mullins effect" refers specifically to the softening observed between the first loading and the subsequent reloadings. However, for the sake of simplicity, many models [42, 43, 44] exclude the difference between unload and reload, and thus come up with a stabilized stress strain curve that has considerably less noise for fitting. The stabilized softening, is often referred to as Idealized Mullins effect [45], and our model is also developed to predict this behaviour.The fundamentals of hydrolysis kinetics and assumptions are first discussed in Section 2. Then, experimental study is presented in Section 3. Next, in section 4, the constitutive model is presented. After a parameter study in section 5, evaluation of the proposed model in comparison to our experimental data and other sets available in literature is presented (section 6). Finally, the summary and discussion is provided in section 7.

2. Hydrolysis Kinetics and Assumptions

Hydrolytic aging results from the interaction of elastomer matrix with the hydroxyl(OH^-) or hydrogen(H^+) ions in water [46]. In general, this process can occur in any media with OH^- or H^+ e.g. acids or alkaline, while the hydrolysis

reaction rate is influenced mainly by ions concentration. Esters, amide, imide, and carbonates are particularly vulnerable to hydrolysis which occurs during water attack. Regardless of the location of those groups in macromolecules, hydrolytic attack of water molecules to those groups can cause chain scission which consequently leads to the production of carboxylic and alcohol end-groups (see eqn.1). Thus aging results in increased concentration of carboxylic end-groups. On the other hand, hydrolytic attack reduces the molecular weight of the matrix, which consequently, influences the mechanical behaviour.

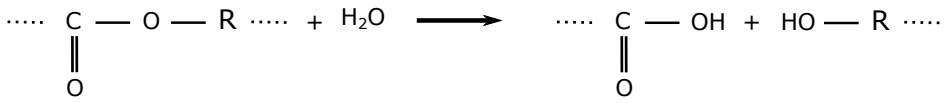

(1)

Kinetic equations are mathematical models to predict and describe a chemical reaction. In this respect, the hydrolysis process can be best modeled via a first order kinetic equation with respect to the carboxylic end groups' formation rate[39]

$$\frac{d[COOH]}{dt} = \zeta[Ester][Water][COOH] = \mathcal{K}[COOH], \tag{2}$$

where $[COOH] = [COOH]_0 \exp(\mathcal{K}t)$. Here, the [Ester],[Water], and [COOH] are the concentration of ester, diffused water, and carboxyl end-groups in the polymer matrix, respectively. The parameter ζ is the hydrolysis constant which defines the rate of hydrolytic attack $\mathcal{K} = \zeta[Ester][Water]$. Here, t is the time variable, and subsequently, we define the subscript $\bullet_0$ to represent the magnitude of a non-kinematic parameter at $t = 0$, e.g. $[COOH]_0$ represents initial concentration of carboxylic group. Since carboxyl end groups concentration is inversely related to number-average molecular weight M_n, one can determine $\mathcal{K}$ by measuring M_n during hydrolytic aging using

$$[COOH] = \frac{1}{M_n} \quad \Rightarrow \quad M_n = M_{n,0} \exp(-\mathcal{K}t). \tag{3}$$

In view of Eq.3, the factors that influence the hydrolysis rate $\mathcal{K}$ are the [Ester], [Water], [COOH] and the hydrolysis constant ζ which itself is a function of temperature, and media's pH, where

- temperature increases the polymer chain mobility and thus increases the ζ [35]
- PH of the degradation environment affects reaction rates through catalysis. and thus increases the ζ [47, 48, 49]

In this study, ζ is assumed to be constant since the temperature, and the PH were kept constant. Accordingly, the proposed model in this work are based on the following assumptions

- The process of water diffusion into the sample is considered to be complete and thus $\frac{d[Water]}{dt} = 0$. In fact, the proposed model is based on the assumption that the water diffusion time t_{diff} inside the sample is significantly smaller than the hydrolytic aging time t_{aging} (i.e. $t_{diff} << t_{aging}$) [50]. The proposed model is mainly relevant for super-thin samples where the assumption of homogeneous diffusion is relevant. Here, we will not investigate in-homogeneous water diffusion due to the sample thickness. Accordingly, all experiments used for validation were performed on super-thin samples (thickness$< 2mm$) that are stored for a duration much longer than a few minutes [51].
- Following completion of water diffusion, the water concentration allover the sample is identical and equal to the maximum saturation level possible $[Water]|_{S \in V} =$ where V represents the sample volume.
- The model is not valid for short time intervals, or ultra thick samples in which $\nabla[Water] \neq 0$ [52].
- Likewise, the concentration of the ester groups $[Ester]$ located at the backbone chains is considered to be almost constant, despite their random scission during the early stages of the aging process [53].

Satisfying the conditions used for the assumption of constant ζ, [Ester] and [water], one can derive the setting at which we can assume $\mathcal{K}$ to be constant. Obviously, this assumption is not relevant in cases where ζ, [Ester] and [water] are non-constant, such as non-uniform water diffusion or varying temperature, and those conditions are not the subject of interest in this work.

3. Experiment

Material: Styrene-butadiene rubber (SBR) procured in rectangular sheets of 24" × 12" × 0.125" were used for validation of the model. The SBR sheets were processed from one batch and provided by one supplier. Standardized dumbbell shape samples were cut from the sheets with a punch die (Die C from the ASTM-D412).

Accelerated aging: Samples were fully immersed in several sealed containers filled with distilled water at temperatures 60°C and 80°C under constant pressure. After a specific aging time, samples were removed and dried at room temperature (i.e. 23°C) for ten day before characterization.

Gravimetric measurement: To measure water-uptake, each sample was individually weighed before and after aging/drying with an accuracy of 0.01mg. Samples were aged in two individual ovens (i.e. 60°C & 80°C) for 1, 10, and 30 days each. Immediately after aging, the samples were carefully dried with a tissue paper and weighed on the same electronic balance. In this respect, the percentage of the water uptake W_C can be written as

$$W_c = \frac{W_t - W_0}{W_0} \times 100 \quad , \tag{4}$$

where W_t and W_0 are the sample weights at time t and virgin state, respectively. Fig. 1a is the plot of the water absorption content versus the square root of hydrolytic aging time for the aging temperature of 60°C. Our data shows that the water uptake is linearly correlated with the square root of aging time (i.e. $W_c \propto \sqrt{t}$), representing that it follows the Fick's second law [54].

In order to investigate the efficacy of the drying process , the aged samples were kept at ambient temperature (i.e. 23°C) and their weights W_{t^*} were recorded at three different drying times t^* (i.e. 3, 5, and 10 days) . For each case, all the weights were then compared with the weight of the virgin sample by substituting W_t with W_{t^*} in Eq.4. Fig. 1b shows the loss of absorbed water along the drying period for two different accelerated aging conditions. The water maintained in the sample reduced exponentially with time and after 10 days, the water content nearly reached its equilibrium value.

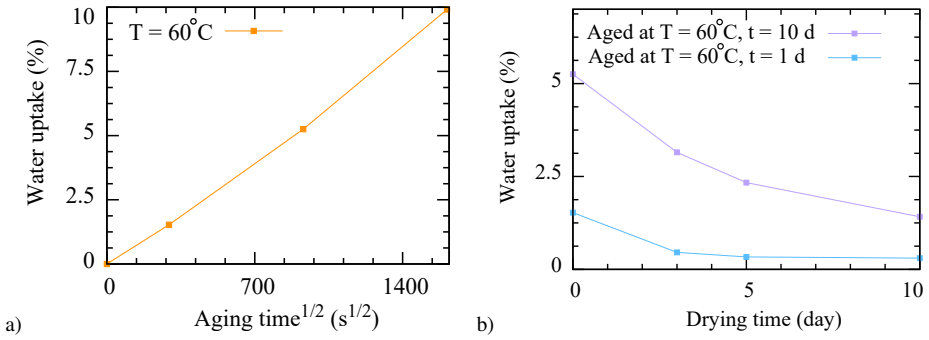

Figure 1: Water content of samples (a) extent of water absorption versus the square root of hydrolytic aging time for 60°C aging temperature, and (b) the loss of absorbed water versus drying time for aged samples.

Mechanical test: United testing machine SFM-20 with a load cell of 1000 lb. was used for quasi-static tensile tests. All tests were displacement controlled with the strain rates of 43.29 $\frac{\%}{min}$. The distance between the machine grips was set to 2.71 inches and all the experiments were performed at room temperature. In monotonic failure tests, the samples were stretched until breakage while in the cyclic test, the samples were stretched to preset amplitudes of 1.3, 1.6, 1.9, and 2.1. Each sample is subjected to a non-relaxing cyclic test with increasing amplitude, where the samples is loaded two times at each amplitudes. In the course of deformation, the elongation of the central zone has been measured by an external extensometer (see Fig. 2). The cyclic experiment is designed to illustrate the evolution of the permanent set and stress softening during the primary loading for both unaged and aged samples.

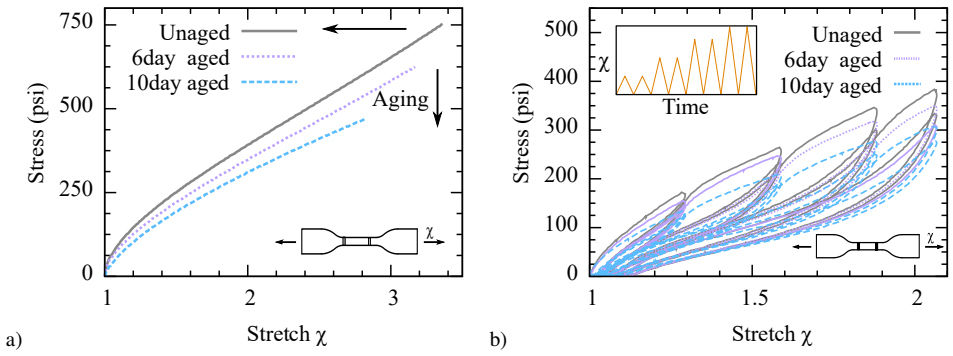

Figure 2: Constitutive behaviour of the dog-bone SBR sample at various aging times shown in (a) failure, and (b) cyclic tests that were performed at 60°C.

Data treatment: The aim of the present work is the modeling of the nonlinear inelastic phenomena such as *permanent set, idealized Mullins effect* during hydrolytic aging. To this end, the experimental data must be treated to highlight the characteristics of these inelastic features. To derive the idealized Mullins effect, the following data treatment will be applied to the experimental data

- The difference between the reloading and unloading curves will be skipped (see Fig. 3a).
- The unloading responses are extended to meet the primary loading that is obtained from the monotonic tensile test. The maximum stress is set to that of the maximum stretch in loading history.

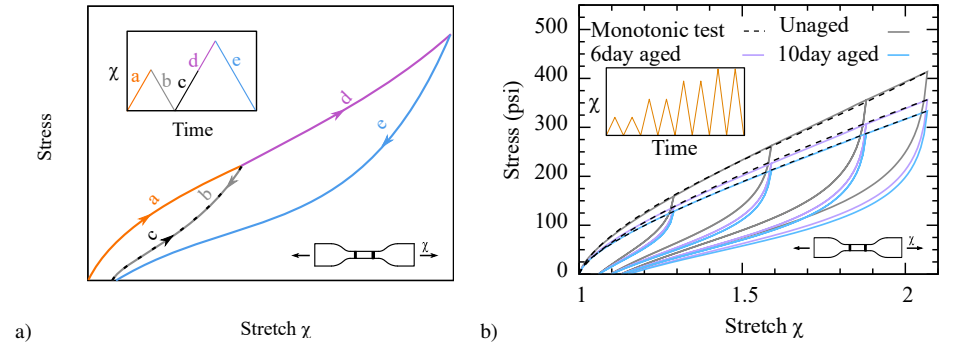

Figure 3: (A) a schematic diagram of idealized Mullins effect, and (b) the treated experimental results of SBR at 60°C for modeling purpose. dashed lines refer to the result of the monotonic tensile tests, while solid lines refer to result of cyclic tests.

The modified experimental results for unaged and aged SBR at 60°C are presented in Fig. 3b. In this figure, the dashed lines refer to the result of monotonic tensile tests and are considered as the primary loading curves. The solid lines are referred to as the secondary curves which correspond to the unloading curves. Each sample experiences a continuous cyclic test regime with increasing stretches in each cycle. The experimental data after the above-mentioned treatment will be used as the basis for the discussion on the modeling of inelastic phenomena such as *idealized Mullins effect and permanent set* in rubber-like material during hydrolytic aging.

4. Constitutive Model

Damage in the polymer matrix should be described with respect to three independent variables temperature T, time t, and deformation which is given by deformation gradient tensor $\mathbf{F}$. To describe the state of damage with respect to time, one can use the status of the matrix at time 0 and ∞ as the reference points and then define a shape function

to interpolate the damage status at time t. Representing the energy of the matrix in the virgin state by Ψ_0 and after indefinite aging time by Ψ_∞, one can approximate the strain energy of the matrix Ψ_M at time t as

$$\Psi_M(t, T, \mathbf{F}) = N(t, T)\Psi_0(\mathbf{F}) + N'(t, T)\Psi_\infty(\mathbf{F}), \tag{5}$$

where $N(t, T)$ and $N'(t, T) = 1 - N(t, T)$ represent the weight of each state. To define the changes of the matrix in the course of hydrolytic aging, one needs to describe the matrix degradation with respect to the shape function N and the energy states Ψ_0, and Ψ_∞. By representing the evolution of the shape function by the Arrhenius function [55], one can write $N(t, T)$

$$N(t, T) = \exp\left(-\gamma \exp(-\frac{E_a}{\mathcal{R}T})t\right), \tag{6}$$

where γ is the degradation constant that defines the rate of hydrolytic aging, E_a the activation energy, and $\mathcal{R} = 8.314[J]/[mol][K]$ the gas constant (see Fig. 4a).

Experimental Derivation of $N(t, T)$ can be carried out through specific relaxation tests, in which samples were aged at constant stretch amplitude for an indefinite time. The changes of the mechanical response from time 0 to ∞ can be associated with the energy states of the material, namely Ψ_0 and Ψ_∞. Having the test results at multiple temperatures, the resulted curves can be used to derive the 3D surface of the $N(t, T)$ directly from the experimental data. *Similar approach can be used in other types of aging including, thermo-oxidative or photo-oxidative.* For example, by considering similar tests that were performed by Johlitz et al [4] on thermo-oxidative aging (see Fig. 4b[2]), one can derive the 3D surface of $N(t, T)$ directly from the experiments (see Fig. 4c). However, in view of the excessive costs associated with relaxation tests, especially in hydrolysis condition, we introduced another approach to approximate $N(t, T)$ based on simpler experiments and a fitting procedure.

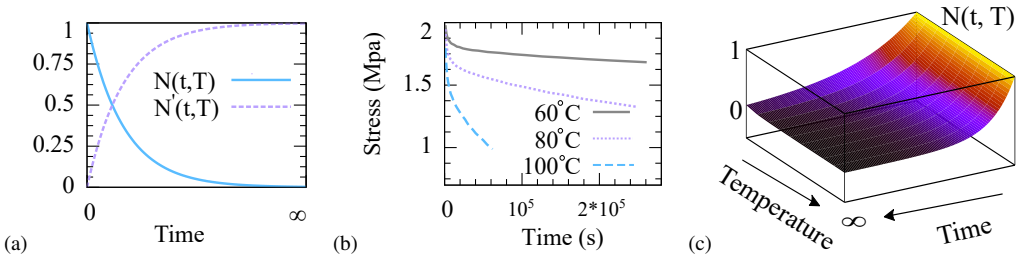

Figure 4: (a) Shape functions in one dimension using Arrhenius function, and (b) Relaxation tests designed to capture the changes in the stress during a deformation controlled aging scenario [4] , and (c) the reconstructed surface of $N(t, T)$.

In matrix of rubber-like materials, the polymer macro-molecules are often cross-linked or bonded to aggregate surfaces at many points along their length. Thus, each macro-molecule has been often bonded at many locations and from multiple polymers strands which are named as "chains" throughout this manuscript [56]. Here, the definition of a chain is considered as the whole or a part of a polymer molecule restricted between two constrained segments, which are either cross-linked or entangled with other chains or alternatively bonded to the aggregate surface. Considering that the length of an active chain is measured between two cross-linked regions along a polymer molecule, the less the cross-link density within a polymeric material, the lengthier the active chains will be. Accordingly, once water attacks the matrix, two parallel phenomena occurs [40] (i) reduction of the cross-links which increases average chain length in the matrix, and (ii) Energy dissipation due to the reduction of polymer active agents. To this end, a fully attacked matrix Ψ_∞ can be decomposed into two independent networks, namely a newly morphed network Ψ_m and a deactivated network Ψ_d as given below

$$\Psi_\infty = \alpha\Psi_m + (1 - \alpha)\Psi_d, \tag{7}$$

where Ψ_m and Ψ_d represent the energies of the morphed and deactivated networks, respectively. The morphed network results from the reduction of the unattacked network cross-links, and consequently, it has chains that are longer than

[2]Data were completed to capture time 0, and the tests were originally performed to capture thermo-oxidative aging.

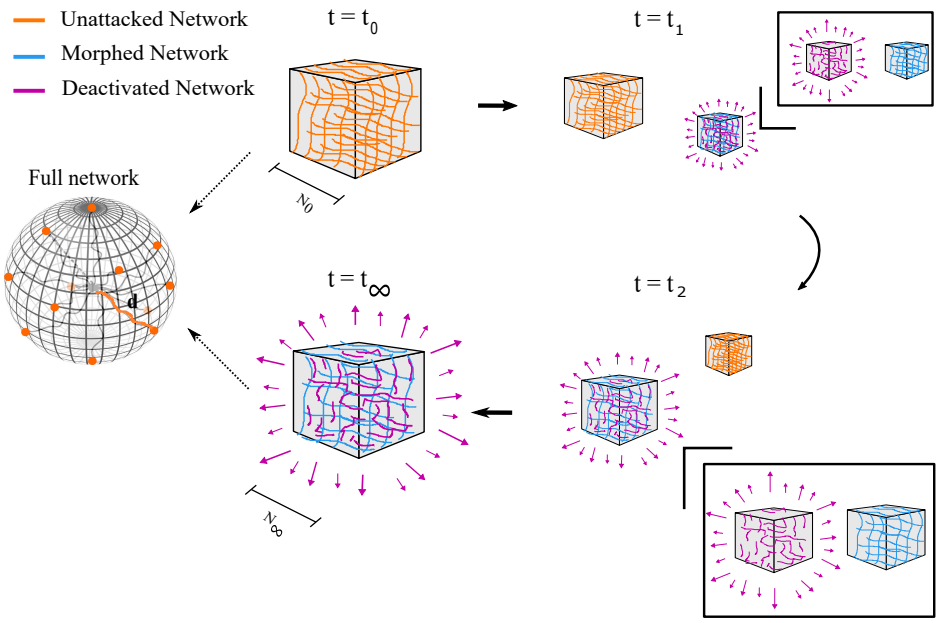

Figure 6: Evolution of the networks throughout hydrolytic aging (cube dimensions represent the number of their chains).

those of the virgin matrix. Moreover, the deactivated network is resulted from water attack to polymer chains. Hence, in this network, the chain length distribution are similar to that of original polymer matrix.

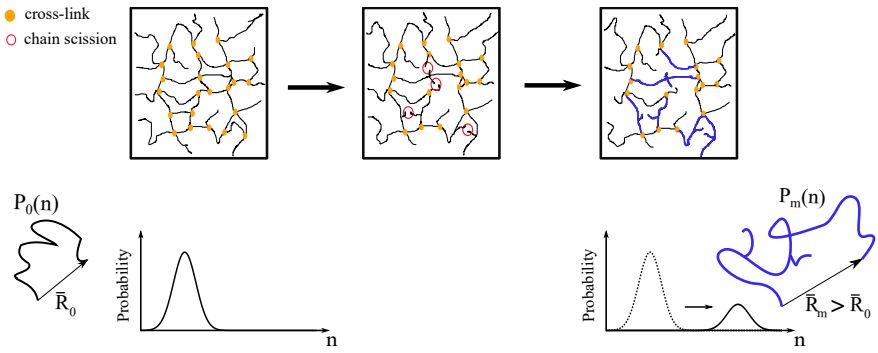

Figure 5: Development of longer chains due to chain scission

The parameter α defines the contribution of each network. Substituting Eq.7 into Eq.5, one gets the total strain energy of the polymer matrix as

$$\Psi_M = N(t,T)\Psi_0 + \alpha\, N'(t,T)\Psi_m + \ (1-\alpha)N'(t,T)\Psi_d. \tag{8}$$

Fig. 6 shows the evolution of the polymer matrix with respect to time. At time $t = 0$, polymer matrix can be represented by Ψ_0 state only. As time passes, contribution of Ψ_∞ grows which itself can be decomposed into two networks, m and d. This process continues until the contribution of Ψ_0 becomes negligible and $\Psi_M \approx \Psi_\infty$.

We assume that all chains which are exposed to water attack within the deactivated network will form free-end chains with no contribution to entropic energy, so $\Psi_d = 0$. So in Eq.8, Ψ_M is mainly determined by the energies of the other two networks, namely Ψ_0 and Ψ_m.

Networks and Subnetworks. Each network is considered to have a unique composition, and describes a specific energy-dissipating damage mechanism. Using the concept of micro-sphere,[57, 58] each network is considered as

a 3D composition of infinite 1D subnetworks that are distributed in all spatial directions. Subnetworks can only be subjected to uniaxial deformation λ, and thus will experience different deformations based on their directions (see Fig. 6)[59, 60]. To develop a model for the subnetwork in direction $\boldsymbol{d}$, only a simplified form of entropic energy is needed, with respect to uni-axial deformation, $\lambda^{\boldsymbol{d}}$. The parameter $\psi^{\boldsymbol{d}}$ represents the energy of the subnetwork in an arbitrary direction, $\boldsymbol{d}$. Integrating a subnetwork in all directions, the consequent network is a representation of that concept in a 3D configuration. Here, by assuming the isotropic spatial distribution of the polymer matrix in reference configuration, the macroscopic energy of an arbitrary network, $\Psi_\bullet$, can be written as

$$\Psi_\bullet = \frac{1}{A_s}\int_S \overset{\boldsymbol{d}}{\psi}_\bullet d\overset{\boldsymbol{d}}{u} \cong \sum_{i=1}^{k} \overset{\boldsymbol{d}_i}{\psi}_\bullet w_i, \quad \Rightarrow \quad \overset{\boldsymbol{d}}{\psi}_M = N(t,T)\overset{\boldsymbol{d}}{\psi}_0 + \alpha N'(t,T)\overset{\boldsymbol{d}}{\psi}_m, \tag{9}$$

where A_s is the surface area of a micro-sphere S, and $u^{\boldsymbol{d}}$ the unit area of the surface with the normal direction $\boldsymbol{d}$. The parameters w_i are weight factors corresponding to the collocation directions $\boldsymbol{d}_i$ ($i = 1, 2, \ldots, k$). A set of $k = 45$ integration points on the half sphere was found to yield the best optimization between computational expenses and the resulted error [61, 62]. Fig. 6 depicts the composition of the polymer matrix into the three networks *0, m* and *d* to describe hydrolysis-induced damages.

Probability Distribution Function of a Polymer Chain. Assuming all subnetworks of each network to have the same composition of chains, one can derive a Gaussian probability function like $\mathcal{P}_\bullet(L|\sigma, \mu_\bullet, R_\bullet)$ which holds for both network [63]. Here, $L = nl$ and $R_\bullet$ represent the contour length and the end-to-end distance of a polymer chain, while $\mu_\bullet$ and σ denote the mean and the standard deviation. Considering n to be the number and l to be the length of the segments, one can normalize L and R by segment length to achieve normalized length $n = \frac{L}{l}$, and $\bar{R}_\bullet = \frac{R_\bullet}{l}$. Moreover, considering $\bar{R}_\bullet$ to be constant in each sub-network, the distribution function can be abstractly written as $\mathcal{P}_\bullet(n) := \mathcal{P}_\bullet(L|\sigma, \mu_\bullet, R_\bullet)$ where

$$\mathcal{P}_\bullet(n) = \frac{1}{2\sqrt{\pi\sigma^2}} \exp\left(\frac{(n-\mu_\bullet)^2}{-2\sigma^2}\right), \tag{10}$$

where the subscript $X_\bullet$ represents the network the parameter X is associated with.

Strain energy of a single chain at networks 0, and m . Based on non-Gaussian theory of rubber elasticity and its approximation through Kuhn-Grün (KG) model, the entropic energy of a single freely jointed chain is given by

$$\psi_c(n, \bar{r}_\bullet) = nK_bT\left(\varphi\beta + \ln\frac{\beta}{\sinh\beta}\right) = nK_bT\int_0^\varphi \beta\, d\varphi, \tag{11}$$
$$\beta = \mathcal{L}^{-1}(\varphi) \quad \text{where} \quad coth(\beta) - \frac{1}{\beta} = \mathcal{L}(\varphi)$$

where $\beta = \mathcal{L}^{-1}(\varphi)$ is the inverse Langevin function, $\varphi = \frac{r_\bullet}{L} = \frac{\bar{r}_\bullet}{n}$ the extensibility ratio ($\frac{\bar{r}_\bullet}{n}$), and $\bar{r}_\bullet$ is end-to-end distance of the chain in the deformed configuration . Recent studies show that the relative error of Kuhn-Grün is significantly large in shorter length ($n < 40$) [64], and can cause significant overs estimation of force in highly cross-linked materials. Therefore, the KG is not a proper option for estimating the entropic energy of matrix with short chains. To this end, an enhanced version of non-Gaussian distribution function of short chains will be used, namely

$$\hat{\psi}_c(n, \bar{r}_\bullet) = nK_bT\int_0^\varphi \hat{\beta} d\varphi, \quad \hat{\beta} = \left[1 - \frac{1+\varphi^2}{n}\right]\beta. \tag{12}$$

Having the same computational cost as the KG model, the enhanced model can provide us with a significantly more accurate description of force in shorter chains.

ILF Approximation. The majority of the micromechanical models either calculate the ILF implicitly, or approximate it with rational functions, as it cannot be explicitly derived. In the whole range of extensibility of polymer chains, it is preferable to approximate the ILF with a highly accurate simple approximation . Thus, a first-order fractional approximation with two polynomial terms (relative error of 1.0%), is used to approximate ILF [65, 66]

$$\mathcal{L}^{-1}(x) \cong \frac{1}{1-x} + x - \frac{8}{9}x^2. \tag{13}$$

4.1. Damage

Damage in the polymer matrix will take place with respect to two main factors: time t and deformation $\mathbf{F}$. Here, we consider temperature to only maximize the rate of damage rather than being an initiating factor in the damage. The time and deformation-induced damages are considered to be taken place in the following forms in networks *0* and *m*

- Time-induced damage is mainly associated to the dissolution of the cross-links in the course of aging which results in homogeneous detachment of polymer chains regardless of their length (random chain scission). Such damage can be best modeled by the changes in the end-to-end distance $\bar{R}_\bullet$ of a polymer chain (see Fig. 7) and the peak location of the distribution function $\mathcal{P}_\bullet(n)$ (see Fig. 5).

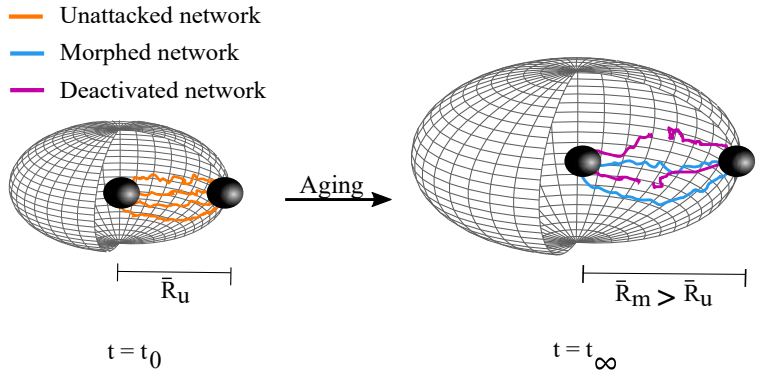

Figure 7: Illustration of time-induced damage due to change of the network morphology

- Deformation-induced damage is mainly associated to the detachment of shorter chains due to entropic force that exceeds the strength of the weakest link of the chain F^{fb}. Such damage results in deactivation of shorter polymer chains and does not have any effects on other longer chains and thus does not change the distribution profile (see Fig. 8).

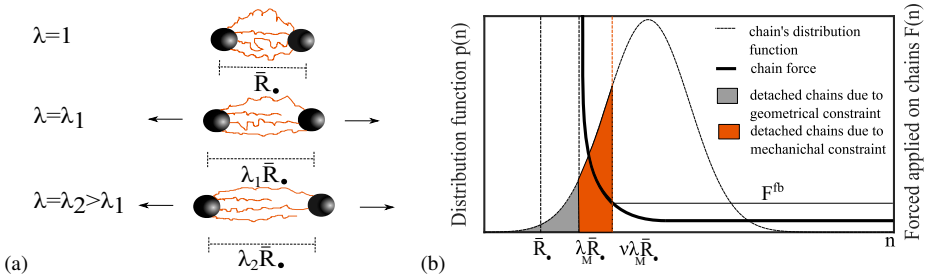

Figure 8: Illustration of deformation-induced Damage. (a) Detachment of shorter chains during primary loading, and (b) Distribution function and the force developed by chains with an equal initial relative end-to-end distance $\bar{R}_\bullet$ and pre-stretched by λ_M

Hence, the shortest available chain in an arbitrary direction of a deformed network is given by

$$F\left(\frac{\bar{r}_\bullet}{n}\right) \leq F^{fb} \quad \longrightarrow \quad n_{\bullet_{min}} = \nu\lambda_M^{\boldsymbol{d}}\bar{R}_\bullet, \tag{14}$$

where ${\lambda_M}^{\boldsymbol{d}}$ is the maximal micro-stretch previously reached in the loading history, while $\nu = \mathcal{L}(\frac{F^{fb}}{K_bT})^{-1} > 1$ refers to a material parameter representing the sliding ratio of a polymer chain (see [67] for details). Considering $n_{\bullet_M} = \mu_\bullet + 5\sigma$ to be the length of longest available chain in each network and use it as a cut-off length of $\mathcal{P}_\bullet(n)$, can significantly reduce the computational cost of the model and eliminate the negligible contribution of super-long chains. Consequently, the length of available chains in the direction $\boldsymbol{d}$ of an arbitrary network is given through the following set

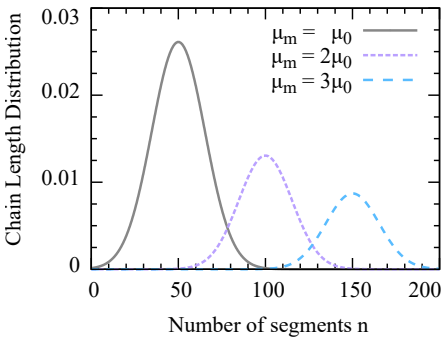

Figure 9: Alteration of the morphed network chain length distribution with respect to the μ_m

$$D_\bullet\left(\begin{matrix}d\\ \lambda_M\end{matrix}\right) = \left\{ n \left| n_{\bullet_{min}}\left(\begin{matrix}d\\ \lambda_M\end{matrix}\right) \leq n \leq n_{\bullet_M} \right\}. \tag{15}$$

4.2. Network Rearrangement

Time-induced Rearrangement . The chain length distribution function $\mathcal{P}_\bullet(n)$ in each network is not a function of time and only its multiplicative amplitude, $N(t,T)$ is evolving over time. Thus, one can show that the total number of bonds at time 0 and ∞ are identical as a result of the conservation of the number of active chains in the matrix. However, the chains of virgin network transformed into the new chains of attacked networks, which can be summarized as follows

$$\begin{aligned} N(0,T)\mathcal{N}_0 \int_{D_0(1)} \mathcal{P}_0(n)\, ndn = N'(\infty,T)\alpha\mathcal{N}_m \int_{D_m(1)} \mathcal{P}_m(n)\, ndn \\ + N'(\infty,T)(1-\alpha)\mathcal{N}_d \int_{D_d(1)} \mathcal{P}_d(n)\, ndn, \end{aligned} \tag{16}$$

where $\mathcal{N}_\bullet$ represents the number of chains in an arbitrary network. Here, one should note that the process of hydrolysis can be defined as the conversion of chains of the virgin network $\mathcal{N}_0$ to the chains of the deactivated and morphed networks $\alpha\mathcal{N}_m + (1-\alpha)\mathcal{N}_d$. In other words, initial polymer chains transform into two states in the course of hydrolytic aging; (i) longer chains formed by merger of original detached chains and (ii) detached chains that could not stay active in the system. Here, we assumed water attacks to the part of chains in the virgin network and deactivate them. Thus, the chain length distribution, $\mathcal{P}_d(n)$ and number of chains, $\mathcal{N}_d$, in the deactivated networks are considered to be the same as the ones ones of the virgin network, $\mathcal{P}_d(n) \approx \mathcal{P}_0(n)$ and $\mathcal{N}_d = \mathcal{N}_0$. Thus, Eq.16 can be rewritten as

$$\begin{aligned} \mathcal{N}_0 \int_{D_0(1)} \mathcal{P}_0(n)\, ndn = \mathcal{N}_m \int_{D_0(1)} \mathcal{P}_m(n)\, ndn \\ \Rightarrow \quad \hat{\mathcal{N}} = \frac{\mathcal{N}_m}{\mathcal{N}_0} = \frac{\int_{D_0(1)} \mathcal{P}_0(n)\, n\, dn}{\int_{D_m(1)} \mathcal{P}_m(n)\, n\, dn}, \end{aligned} \tag{17}$$

where $\hat{\mathcal{N}}$ is a normalization constant, which satisfy the mass conservation in the networks during aging time.

In this respect, Fig. 9 shows the alteration of the chain distribution function due to the change of $\mathcal{N}_m$ with respect to μ_m in the morphed network. By increasing μ_m, $\mathcal{N}_m$ decreases and moves the distribution function to the right and down (See Fig. 9).

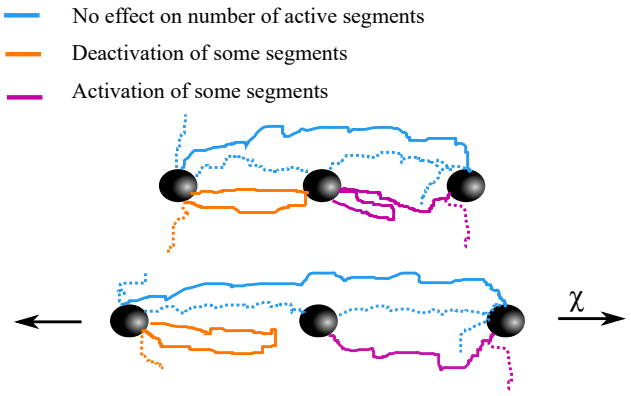

Figure 10: Effect of chain detachment on the number of active segments.

Deformation-induced Rearrangement . Considering that the detached chains still remain part of a longer macro-molecules, two presumptive conclusions can be made; (i) the detachment of the chains does not lead to full dissipation of their energy, and (ii) the number of active segments within a network remains constant in the course of deformation (see e.g. To implement this assumption, we consider the detached chains to be evenly distributed among available chains and thus increase the number of active chains, though with the same probability function $\mathcal{P}_\bullet(n)$. Accordingly, in the course of primary loading shorter chains detach and become part of the longer chains (see Fig. 10). In the unloading and reloading no further damage occurs, as long as λ_M remains the same. [67, 68] for details). The network rearrangement can be best quantified through an amplification factor $\Phi_\bullet(\lambda_M)$ which amplifies the distribution profiles $\mathcal{P}_\bullet(n)$ as more chains are detached from the matrix [69]. This process can take place in m or 0 networks depending on the λ_M on that direction. Assuming the number of segments to be identical before and after deformation, one can write

$$\mathcal{N}_\bullet \Phi_\bullet(1) \int_{D_\bullet(1)} \mathcal{P}_\bullet(n)\, ndn = \mathcal{N}_\bullet \Phi_\bullet(\lambda_M) \int_{D_\bullet(\lambda_M)} \mathcal{P}_\bullet(n)\, ndn. \tag{18}$$

The detachment process is irreversible; we consider no new bonds to be formed during reloading and unloading, and thus one can rewrite Eq. 18 by considering $\Phi_\bullet(1) = 1$ as

$$\Phi_\bullet(\lambda_M) = \frac{\int_{D_\bullet(1)} \mathcal{P}_\bullet(n)\, ndn}{\int_{D_\bullet(\lambda_M)} \mathcal{P}_\bullet(n)\, ndn}. \tag{19}$$

4.3. Strain Energy of Networks

The free energy of networks 0 and m in an arbitrary direction $\boldsymbol{d}$ can be written with respect to Eqs. 12, 17, and 19

$$\overset{\boldsymbol{d}}{\psi}_\bullet = \int_{D_\bullet\left(\lambda_M \boldsymbol{d}\right)} \Phi_\bullet\left(\overset{\boldsymbol{d}}{\lambda}_M\right) \psi_c(n, \bar{r}_\bullet)\, \mathcal{P}_\bullet(n)\, dn, \tag{20}$$

where $D_\bullet$ represents the available chains' length in $\bullet^{th}$ network.

Micro-Macro Scale Transition is used to define the relationship between the micro and macro deformation within the polymer matrix. Here, *the non-affine directional model* is used to relate the macro-stretch χ, and the micro-stretch λ. Based on this concept, a non-homogenous distribution of the stretch within the network domain is assumed. Here, a

classical strain amplification function which is often used in rubber-like materials [70, 71] is used, however the model can be changed for polymers with more elaborate behaviour.

$$\overset{\boldsymbol{d}}{\lambda} = \frac{\chi^{\boldsymbol{d}} - C^p}{1 - C^p} \tag{21}$$

where $C \in [0, 1]$ is the volume fraction of hard segments per unit volume of the rubber matrix, and p depends on the structure of the network ($p \approx 1/3$ for details see [72]).

4.4. Constitutive formulation

For an incompressible polymer matrix

$$\det \mathbf{F} = 1 \tag{22}$$

where $\mathbf{F}$ stands for the macro-scale deformation gradient. The first Piola-Kirchhoff stress tensor P can be written as

$$\mathbf{P} = \frac{\partial \Psi_M}{\partial \mathbf{F}} - p\mathbf{F}^{-T} = \frac{\partial \Psi_0}{\partial \mathbf{F}} + \frac{\partial \Psi_m}{\partial \mathbf{F}} - p\mathbf{F}^{-T}, \tag{23}$$

where p denotes an arbitrary scalar parameter which can be defined to assure incompressibility, and

$$\begin{aligned}
\frac{\partial \Psi_0}{\partial \mathbf{F}} &= N(t,T) \sum_{j=1}^{k} w_j \frac{\partial \overset{\boldsymbol{d}}{\psi}_0}{\partial \overset{\boldsymbol{d}_j}{\lambda}} \frac{\partial \overset{\boldsymbol{d}_j}{\lambda}}{\partial \overset{\boldsymbol{d}_j}{\chi}} \frac{1}{2\overset{\boldsymbol{d}_j}{\chi}} \frac{\partial \boldsymbol{d}_j \bar{\mathbf{C}} \boldsymbol{d}_j}{\partial \bar{\mathbf{F}}} : \frac{\partial \bar{\mathbf{F}}}{\partial \mathbf{F}}, \\
\frac{\partial \Psi_m}{\partial \mathbf{F}} &= \alpha N'(t,T) \sum_{j=1}^{k} w_j \frac{\partial \overset{\boldsymbol{d}}{\psi}_m}{\partial \overset{\boldsymbol{d}_j}{\lambda}} \frac{\partial \overset{\boldsymbol{d}_j}{\lambda}}{\partial \overset{\boldsymbol{d}_j}{\chi}} \frac{1}{2\overset{\boldsymbol{d}_j}{\chi}} \frac{\partial \boldsymbol{d}_j \bar{\mathbf{C}} \boldsymbol{d}_j}{\partial \bar{\mathbf{F}}} : \frac{\partial \bar{\mathbf{F}}}{\partial \mathbf{F}},
\end{aligned} \tag{24}$$

where $\mathbf{C}$ denotes the right Cauchy–Green tensor, $J^2 = \det \mathbf{C}$, and $\bar{\mathbf{C}} = J^{-2/3}\mathbf{C}$. Detailed description of the derivation procedure of each of the terms of Eq. 24 has been provided in Appendix A.

5. Parameters Study

Parameter study is carried out to evaluate the contribution of the physical parameters and validate the properties associated with them. First, a reference set of values is selected for all parameters which is given in Table 1. The values are specifically chosen to provide high resolution in material behavior during the aging time (See Fig. 11). To investigate the effects of each parameter on model predictions, we investigate the increased and decreased values of that parameter while all others are kept constant. In view of different effects of parameters at different aging times, we investigated each parameter at three different times, namely $t = 0$, $t = t_1$, and $t = \infty$.

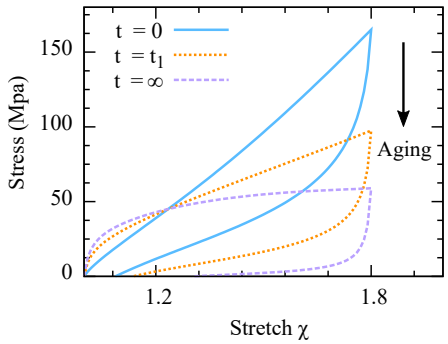

Figure 11: Model prediction with the selected material parameters during the aging time.

Table 1: The reference set of parameters of the proposed model.

$\mathcal{N}_0 k_b T[Mpa]$	$\bar{R}_0$	$\bar{R}_m$	μ_0	μ_m	σ	ν	α	$\gamma \exp(-\frac{E_a}{\mathcal{R}T})$
40	3	18	13	15	4.5	1.0065	0.02	0.1

The proposed model has ten material parameters, four represents the behaviour of unchanged network ($\bar{R}_0$, μ_0, σ, and ν), five those of morphed network ($\bar{R}_m$, μ_m, α, E and γ), and one parameter namely $\mathcal{N}_0$ just serves as a multiplication factor to describe the response of the polymer matrix. Due to similarity of the effect of $\frac{E_a}{\mathcal{R}T}$ and γ on the response of the material in a constant aging temperature, here, we only investigate the variation of $\gamma \exp(-\frac{E_a}{\mathcal{R}T})$ as a rate of aging. In order to analyze the parameters, first, the effect of unchanged network parameters are investigated along the aging trajectory. Fig. 12 shows a summary of the parametric analysis of ($\bar{R}_0$, μ_0, σ, ν, α, and $\gamma \exp(-\frac{E_a}{\mathcal{R}T})$) during aging time.

- **Parameter** $\bar{R}_0$, which represents the end-to-end distance of unchanged network, governs the minimum available chain length ($n_{0_{min}} = \nu \lambda_M \bar{R}_0$) in the unattacked network in any arbitrary direction. Thus by increasing $\bar{R}_0$, $n_{0_{min}}$ increases while the mean length of polymer chains in the network, which is governed by μ_0, remains constant. As shown in Fig. 12a, decreasing $\bar{R}_0$ decreases the inelastic effects such as the hysteresis ratio. As expected, the effects of $\bar{R}_0$ on material response diminishes along aging time since contribution of Ψ_0 becomes negligible .

- **Parameter** μ_0 defines the peak of chain distribution, $P_0(n)$, and can be represented as a multiplicative factor of $\bar{R}_0$. In virgin material, μ_0 plays a significant role in defining the evolution of damage. Accordingly, the damage will increase when $\bar{R}_0$ reaches the peak of probability, μ_0 (see Fig. 12b) as the network loses more chain due to deformation. In addition, this parameter control the number of chain in the morphed network through the normalization constant, $\mathcal{N}_m$. Thus, response of the material will change along the aging time. It is shown (Fig. 12b) that by increasing the μ_0 the softening of material response decreases at $t = 0$ and increases at $t = \infty$.

- **Parameters** σ defines the variance of of chain distribution, $P_\bullet(n)$, and thus have a direct effect on the amount of damage the material experience during deformation. Regardless of aging time, higher values of σ represents wider distribution and consequently lower damage as shown in figures see Fig. 12c.

- **Parameter** v governs the magnitude of energy dissipation in detachment of a chain, and thus the hysteresis ratio and also the profile of the unloading curves. Regardless of aging time, lower values of v represents higher energy dissipation per chain and consequently results in stronger and yet more damageable networks as shown in Figures 12d.

- **Parameter** α defines the composition of the transformed matrix, in particular it is correlated with the percentage of the polymers that transform into m and inversely correlated with those that transform into d networks. Considering the zero contribution of the d network in energy of the matrix, parameter α can be considered as a multiplicative scaling factor for Ψ_m that can linearly scale the contribution of morphed network. As expected, the contribution of α in the final response increases over time as Ψ_m grows with aging as shown in Fig. 12e.

- **Parameter** $\gamma \exp(-\frac{E_a}{\mathcal{R}T})$, or the hydrolysis constant, mainly governs the decay rate of the *0* network and formation rate of the m network. Higher values of $\gamma \exp(-\frac{E_a}{\mathcal{R}T})$, thus, represents a faster transformation from *0* to m networks (See Fig. 12f).

6. Validation and Results

To validate the proposed model, its predictions were bench-marked against a set of new experimental data specifically designed to capture the effects of **(1) deformation** χ**, (2) deformation history** χ_M**, (3) aging time** t **and (4) aging temperature** T. Hereafter, t refer to the time that samples were aged before inducing the deformation χ. The model was optimized by fitting the aforementioned ten material parameters to the following set of load-unload curves

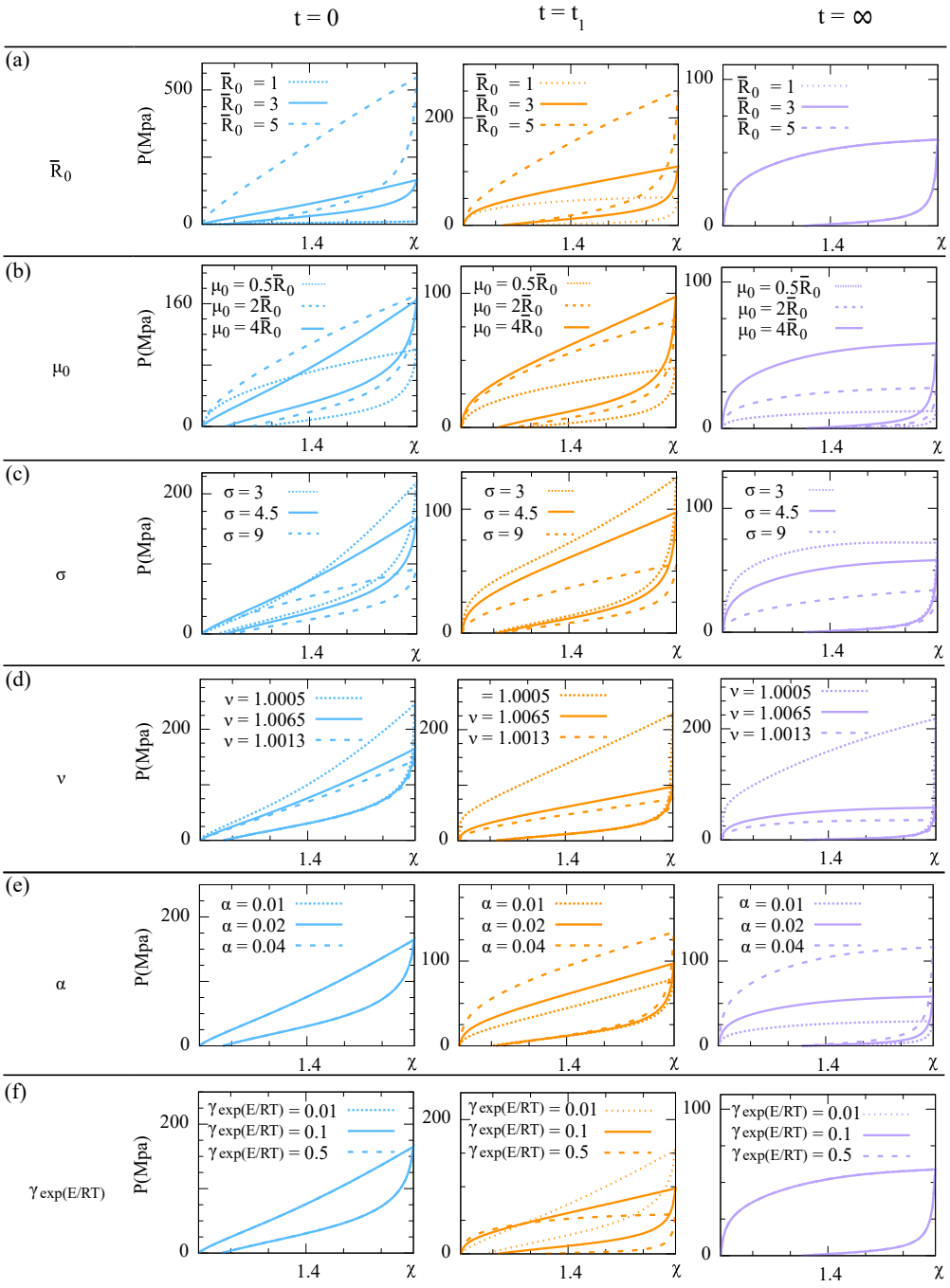

Figure 12: Sensitivity analysis of the material parameters included in the model. Each plot consists of three independent lines. Solid lines represent the reference curve, and dashed lines depict model predictions due to the variation of the control parameters. In some cases, all three lines are on top of each other.

- Primary loading curve of the unaged sample, to study χ
- One unload cycle of the 1.3 stretch amplitude of the unaged sample, to study χ_M
- Only loading curve of 10 days aged sample at 80°C, to study χ, χ_M, and t
- One point: stress at 1.5 stretch for 6 days aged sample 60°C, to study t, and T

To this end, the least square error function was minimized with the aid of the Levenberg–Marquardt algorithm. Once the material parameters are obtained, the model can predict the other loading-unloading curves of materials for a different amount of aging times and strains. In this regard, the model predictions are validated against our own experimental tests for different aging times and temperatures in Fig. 13, while the obtained values of the material parameters are given in Table 2.

Here, we validate the model predictions on different types of damages as given below

- Fig. 13a: Damages induced by deformation, and deformation history in multiple cycles
- Fig. 13b: Damages induced by time and temperature in one cycle
- Fig. 13c and d: Effect of time on damages induced by deformation, and deformation history in multiple cycles
- Fig. 13e and f: Effect of temperature on damages induced by deformation, and deformation history in multiple cycles

Table 2: Material parameters of the proposed model for SBR

$\mathcal{N}_0 k_b T[psi]$	$\bar{R}_0$	$\bar{R}_m$	μ_0	μ_m	σ	ν	α	$\gamma[1/day]$	$\frac{E_a}{\mathcal{R}}$[K]
95.4	3.0547	3.3849	7.04	7.24	7.28	1.0055	0.001	1459	3700

Moreover, to quantify the deformation-induced damages of polymers in the course of hydrolytic aging, the dissipated energy in each cycle in the model is predicted and compared to those of the experimental data. Throughout this contribution, the term "Hysteresis" will be used to refer to "quasi-static" energy dissipation observed in one load-unload cycle in uni-axial tensile tests. In elastomers, while hysteresis is strongly dependent on deformation rate, even at close to zero rates, certain hysteresis can be observed which is referred to as rate-independent or "quasi-static" hysteresis. We generally refer to the hysteresis of the first cycle as idealized Mullins effect, while those of the second and next cycles are referred to as hysteresis. Please note that this "Hysteresis" is different than frequency dependent visco-elastic hysteresis since this one is resulted by a combination of reversible and irreversible energies observed in quasi-static loading as the result of sub-structural damages such as bond detachments. At any aging time t and temperature T, the dissipated energy per unit of volume during the first cycle can be calculated from the experiments as follows

$$U_{hys}{}^{t,T} = \int_{loading} \mathbf{P}^{t,T}\boldsymbol{X} \otimes \boldsymbol{X} d\chi - \int_{unloading} \mathbf{P}^{t,T}\boldsymbol{X} \otimes \boldsymbol{X} d\chi, \tag{25}$$

where $\boldsymbol{X}$ is the deformation vector applied on the matrix. Fig. 14 show the evolution of dissipated energy against χ_M for different aging times at 60°C, and 80°C, respectively. As expected, the dissipated energy increases exponentially with χ_M while the growth rate is being inversely correlated to aging time t.

Considering the micromechanical nature of the mode, the concept can be further generalized and implemented for other types of cross-linked polymers with *complex inelastic patterns such as hardening behavior and alteration of curvature*. Here, we generalized the model to predict the hydrolytic aging behavior of three other compounds form experimental data that are available in literature

- Polyurethane [73]

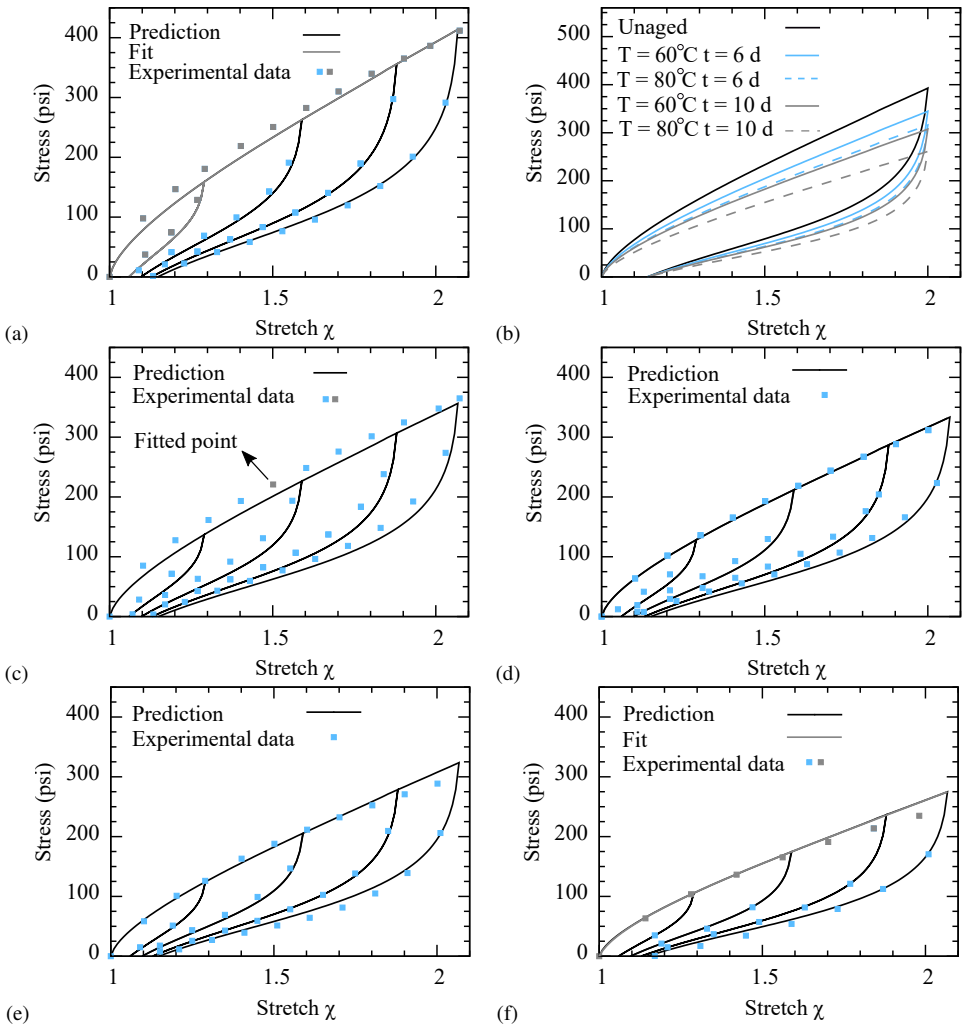

Figure 13: Validation of model predictions for SBR in multiple conditions; (a) unaged, (b) Comparison of one cycle load on samples stored at 60°C and 80°C for 6 and 10 days, (c) constitutive behaviour for 6 days aged sample at temperature 60°C, (d) constitutive behaviour for 10 days aged sample at temperature 60°C, (e) constitutive behaviour for 6 days aged sample at temperature 80°C, (f) constitutive behaviour for 10 days aged sample at temperature 80°C.

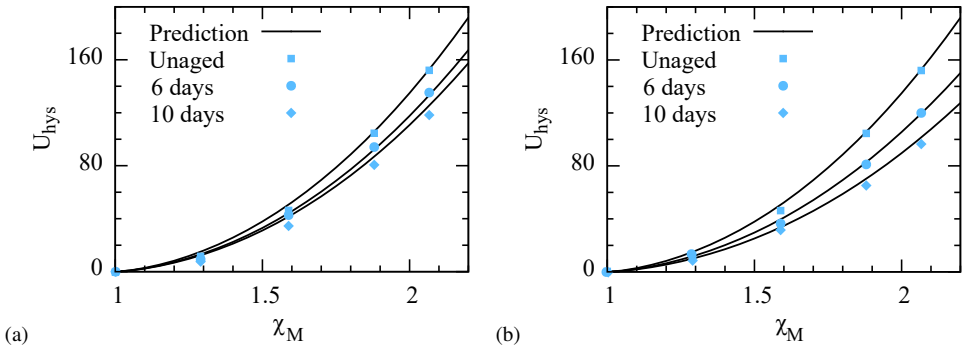

Figure 14: Evolution of dissipated energy during aging at different temperatures; (a) 60°C, (b) 80°C

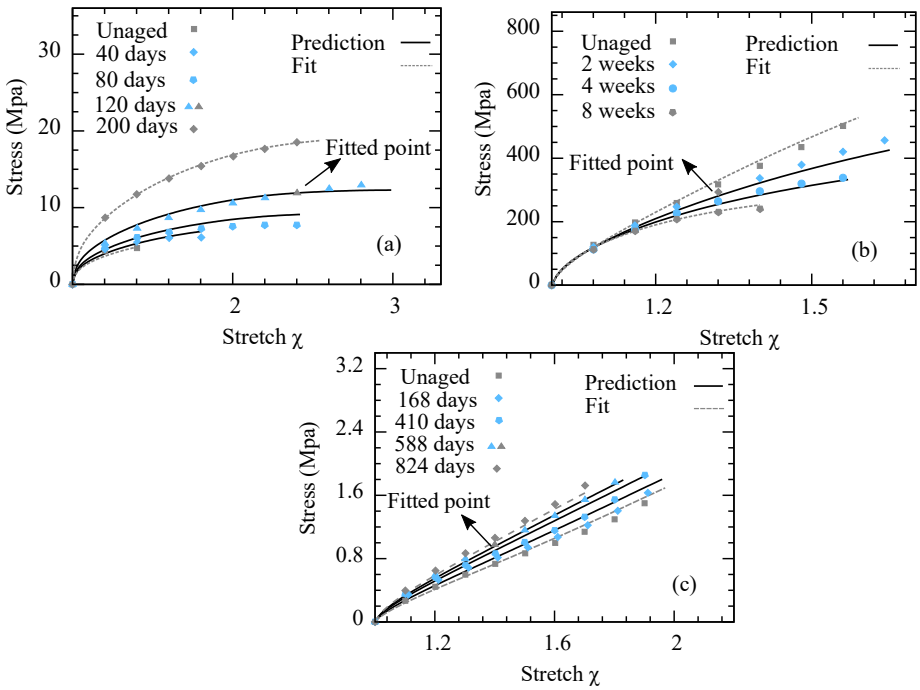

Figure 15: Validation of model predictions against aging of three different materials; (a) PolyUrethane (PU) submerged in seawater at 100°C[73], (b) PLA–PCL fiber submerged in phosphate buffer solution at 37°C[35], (c) Natural rubber (vulcanized A) submerged in seawater at 40°C [74]

- Suture fibers of PLA–PCL[35]
- Natural rubber[74]

To fit the parameters for each material, two loading curves of unaged and aged samples, as well as one point of an additional loading curve from another sample with a different aging period were considered for fitting. The parameters for each of the above mentioned materials are derived and summarized in Table 3. In this table, the decay constant $\gamma \exp(-\frac{E_a}{\mathcal{R}T})$ presented as single parameter as material responses captured only in one temperature. Fig. 15 shows the predictive capabilities of the presented model against the experiments for all three materials, and the good agreement for rest of curves were obtained automatically.

Table 3: Material parameters of the proposed model for different Set of rubber-like materials

Ref.	$\mathcal{N}_0 k_b T$ $[Mpa]$	$\bar{R}_0$	$\bar{R}_m$	μ_0	μ_m	σ	ν	α	$\gamma \exp(-\frac{E_a}{\mathcal{R}T})$ $[1/day]$
Gac et al.[73]	0.32	13.374	17.535	5.5	7.5	5.1	1.005	0.3	0.0209
Vieira et al.[35]	4.88	10.567	21.795	13.04	15.5	4.28	1.01	0.128	0.0443
Stevenson.[74]	0.13	6.027	12.582	17.04	19.04	8.28	1.055	0.36	0.001

Depending on the polymer matrix, we assume that **all chains** which are exposed to water attack within the **deactivated network** will form free-end chains, which will have no further contribution to entropic energy. Accordingly, the ratio of morphed network to deactivated network α describes how the matrix elasticity is perceived at time ∞. In this work, we assume that α has been inversely correlated to Ψ_∞, so for $\alpha = 0$ we expect the material to show no retention force at time ∞, and for $\alpha = 1$ we expect the system to remain fully elastic. Since SBR loses most of its elasticity due to hydrolysis, the response can be simply described by transformation of the virgin network to the deactivated network with almost negligible contribution of morphed network $\alpha \approx 0$. Hence, the energy at infinity

state can be considered zero (i.e. $\Psi_\infty = 0$) which shows that the material will be annihilated through aging. However, for other type of the material such as polyurethane which retain elasticity at time ∞, α will remain relatively high and $\Psi_\infty = \alpha\Psi_m$.

Using micro-sphere as the basis of deactivated and morphed networks in our model, the proposed model can be independently used to predict aging in different mechanical loading scenarios. Once the model has been fitted to uni-axial data, its predictions were validated against shear and uni-axial tensile loads in virgin-state (see Fig. 16). While we did not find data on the multi-axial performance of elastomeric samples under hydrolytic aging, model predictions on the aging of samples under different loading were predicted but only validated with respect to uni-axial loading. Using the data of [75] on uni-axial and pure shear of filled silicone rubber, the proposed model validated for different loading scenarios in Fig.16. For the fitting, we used one loading-unloading cycle of the 1.413 stretch amplitude in the uni-axial tensile direction. The good agreement with all loading-unloading curves in pure shear, as well as other loading-unloading curves of uni-axial tensile, was attained automatically. The obtained values of the material parameters are given in Table 4.

Table 4: Material parameters of the proposed model for filled silicone rubber

Ref.	$\mathcal{N}_0 k_b T$ $[Mpa]$	$\bar{R}_0$	$\bar{R}_m$	μ_0	μ_m	σ	ν	α	γ $[1/day]$	$\frac{E_a}{\mathcal{R}}$ [K]
Machado et al.[75]	0.2858	2.0640	4.25	13.04	15.04	6.28	1.004	0.04	1759	3700

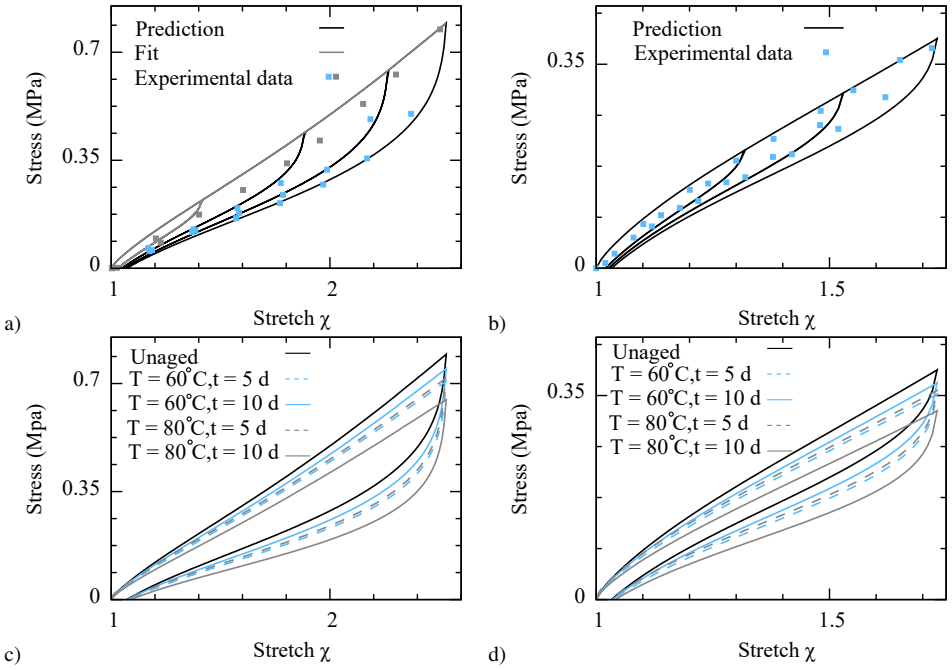

Figure 16: Validation of model predictions for silicone rubber under different loading scenarios against experimental data from [75]; (a) unaged sample under uni-axial tension, (b) unaged sample under pure shear, (c) Comparison of one cycle of uni-axial tension load on samples stored at 60°C and 80°C for 5 and 10 days, (d) Comparison of one cycle of pure shear load on samples stored at 60°C and 80°C for 5 and 10 days.

7. Summary and Discussion

We have developed a large strain three-dimensional micro-mechanical constitutive model to describe the hydrolytic aging of a cross-linked polymers matrix with permanent chemical cross-links that can break and reform the

matrix with respect to four external load factors of (i) deformation, (ii) deformation history, (iii) aging time and (iv) aging temperature. Our model show excellent agreements with the experimental data on five different types of loading and on four different materials. To the best of our knowledge, this is the first micromechanical model of hydrolytic aging.

The model has been based on the concept that the chemical cross-links can break, can consequently transform the network in the course of aging. We hypothesized two different types of network transformation depending on the source of cross-link breakage, namely time or deformation. During a test with continuous loading, the deformation-induced damage will lead to detachment of shorter chains and thus results in a rearranged network with slightly longer polymer chains. In the course of aging and in the absence of deformation, we assume that the chain detachment due to water attack on polymer active agents occurs randomly and thus the reformed network will have a different composition from the original network with fewer chains. Rearrangement of the chains contributes significantly to the overall stress of the cross-linked polymer matrix and was accurately represented by our model. Although our model has ten independent parameters, two of them can be immediately eliminated if deformation controlled relaxation aging tests are available. Here, Our formulation neglects rate dependency and viscoelasticity while the major focus of this work is on relatively long aging times and low deformation rates where the effects of viscoelasticity is assumed to disappear. Thus, if the deformation rate is sufficiently low one can assume the tests, pre- and post-aging, as quasi-static tests which makes the unloading curves insensitive to the loading rate and mainly a function of deformation history.

The proposed model captures the basic physical laws governing the hydrolytic aging of cross-linked polymers as frequently encountered in nature and thus is relevant to to other types of chemically crosslinked polymers such as rubber-like materials, adhesives and sealants. For polymeric systems with more complex morphology, e.g. those with two or more types of cross-links or polymers, while the proposed concepts are still relevant, the models describing the dynamics of breaking of cross-links and network rearrangement should be updated and probably, would be way more complex than those used in this work. The proposed model has ten material parameters, all of which have a clear physical meaning. The excellent performance of the proposed method was proven by validating against different experimental data on different materials that are particularly selected to reveal the evolution of inelastic behaviour during hydrolytic aging. The model predictions was further validated by comparing the evolution of hysteresis against experiments. Our model and experiments illustrate how polymer networks with their mechanical behaviour dominated by entropic chains, can respond to time, temperature and deformation at the micro-structural level and further explore the relation to describe macroscopic response with respect to micro-structural changes.

Acknowledgments

This material is based upon work supported by the U.S. Department of Energy's Office of Energy Efficiency and Renewable Energy (EERE) under the Award Number DE-EE0008455.

Disclaimer

Appendix A. Energy Derivatives

The terms of Eq.24 can be further simplified by means of the following identities

$$\frac{\partial \psi_c\left(n, x\bar{R}\right)}{\partial x} = \bar{R}K_B T\hat{\beta}\left(\frac{x\bar{R}}{n}, n\right), \tag{A.1}$$

$$\frac{\partial \psi^{\boldsymbol{d}}{}_0}{\partial \lambda^{\boldsymbol{d}_j}} = \mathcal{N}_0 N(t,T)\Phi\left(\overset{\boldsymbol{d}_j}{\lambda}_M\right) \int\limits_{D_n{}^0(\lambda^{\boldsymbol{d}_j}{}_M)} \mathcal{P}_0(n)\left.\frac{\partial \psi_c(n,x)}{\partial x}\right|_{x=\lambda^{\boldsymbol{d}_j}} dn, \tag{A.2}$$

$$\frac{\partial \psi^{\boldsymbol{d}}{}_m}{\partial \lambda^{\boldsymbol{d}_j}} = \alpha\mathcal{N}_m N'(t,T)\Phi\left(\overset{\boldsymbol{d}_j}{\lambda}_M\right) \int\limits_{D_n{}^m(\lambda^{\boldsymbol{d}_j}{}_M)} \mathcal{P}_m(n)\left.\frac{\partial \psi_c(n,x)}{\partial x}\right|_{x=\lambda^{\boldsymbol{d}_j}} dn, \tag{A.3}$$

$$\frac{\partial \lambda^{\boldsymbol{d}_j}}{\partial \chi^{\boldsymbol{d}_j}} = \frac{1}{1-C^p}, \tag{A.4}$$

$$\frac{\partial \boldsymbol{d}\bar{\mathbf{C}}\boldsymbol{d}}{\partial \bar{\mathbf{F}}} : \frac{\partial \bar{\mathbf{F}}}{\partial \mathbf{F}} = 2\bar{\mathbf{F}}(\boldsymbol{d}\otimes\boldsymbol{d}) : J^{-\frac{1}{3}}\mathbb{I} = 2J^{-\frac{1}{3}}\bar{\mathbf{F}}(\boldsymbol{d}\otimes\boldsymbol{d}). \tag{A.5}$$

In the Eq. A.1, $\hat{\beta}$ is the modified version of Langevin elastic force for a short chain. Thus, Eq. 23 yields

$$\mathbf{P} = \frac{K_B T}{1-C^p}\sum_{i=1}^{k}\left[\mathcal{N}_0 N(t,T)P_0(\boldsymbol{d}_i) + \alpha\mathcal{N}_m N'(t,T)P_m(\boldsymbol{d}_i)\right]\frac{w_i}{\overset{\boldsymbol{d}_i}{\lambda}} J^{-\frac{1}{3}}\bar{\mathbf{F}}(\boldsymbol{d}_i\otimes\boldsymbol{d}_i), \tag{A.6}$$

where

$$P_0(\boldsymbol{x}) = \Phi\left(\overset{\boldsymbol{x}}{\lambda}_M\right) \int\limits_{D_{n_0}\left(\overset{\boldsymbol{d}}{\lambda}_M\right)} \mathcal{P}_0(n)\,\mathcal{L}^{-1}(\varphi)\left(1-\frac{1+\varphi^2}{n}\right)dn, \qquad \varphi = \frac{\overset{\boldsymbol{x}}{\lambda}\bar{R}_0}{n}$$

$$P_m(\boldsymbol{x}) = \Phi\left(\overset{\boldsymbol{x}}{\lambda}_M\right) \int\limits_{D_{n_m}\left(\overset{\boldsymbol{d}}{\lambda}_M\right)} \mathcal{P}_m(n)\,\mathcal{L}^{-1}(\varphi)\left(1-\frac{1+\varphi^2}{n}\right)dn, \qquad \varphi = \frac{\lambda^{\boldsymbol{x}}\bar{R}_m}{n} \tag{A.7}$$

Appendix B. Thermodynamic Consistency

Since the strain energy of the polymer matrix Ψ_M is influenced by only one internal variable, namely $\overset{\boldsymbol{d}}{\lambda}_M$, one can rewrite Ψ_M as

$$\Psi_M = \Psi_M(\bar{\mathbf{C}}, \boldsymbol{\Lambda_M}) = \tilde{\Psi}_M(\bar{\mathbf{F}}, \boldsymbol{\Lambda_M}) = \Psi_o(\bar{\mathbf{C}}, \boldsymbol{\Lambda_M}) + \Psi_m(\bar{\mathbf{C}}, \boldsymbol{\Lambda_M}), \tag{B.1}$$

where

$$\boldsymbol{\Lambda_M} = \left\{\overset{\boldsymbol{d}}{\lambda}_M : \boldsymbol{d}\in\mathbb{V}^3 \wedge |\boldsymbol{d}| = 1\right\}. \tag{B.2}$$

The second law of thermodynamics can be reduced to the Clausius-Duhem inequality to show the thermodynamic consistency of the model in an arbitrary direction $\boldsymbol{d}$ [76]

$$\underset{\lambda_M}{\partial_{\boldsymbol{D}}}\,\Psi_M \cdot \left(\overset{\boldsymbol{D}}{\dot{\lambda}}_M\right) \leq 0 \qquad\qquad \forall\, \boldsymbol{d}. \tag{B.3}$$

The maximum stretch remains constant during unloading and reloading. Hence, $\dot{\lambda}_M^{\boldsymbol{d}} = 0$ in unloading-reloading while $\dot{\lambda}_M^{\boldsymbol{D}} > 0$ in the primary loading. Thus, the Clausius–Duhem inequality is satisfied if during the primary loading, the following inequality:

$$\frac{\partial \Psi_M}{\partial \lambda_M^{\boldsymbol{d}}} \leq 0 \qquad \forall\, \boldsymbol{d} \tag{B.4}$$

With respect to Eq.9, Eq.B.3 yields

$$\frac{\partial \Psi_M}{\partial \lambda_M^{\boldsymbol{d}}} = \frac{\partial \Psi_0^{\boldsymbol{d}}}{\partial \lambda_M^{\boldsymbol{d}}} + \frac{\partial \Psi_m^{\boldsymbol{d}}}{\partial \lambda_M^{\boldsymbol{d}}} \leq 0 \;\forall\, \boldsymbol{d}. \tag{B.5}$$

If each term of the (B.5) be less or equal to zero separately, the Clausius-Duhem inequality will be satisfied. First, let's consider the case of $\frac{\partial \Psi_0^{\boldsymbol{d}}}{\partial \lambda_M^{\boldsymbol{d}}}$. Generally, (B.5) can be proved for an arbitrary direction $\boldsymbol{d}$ of primary loading. For the sake of simplicity, $\lambda_M^{\boldsymbol{d}}$ and $\lambda^{\boldsymbol{d}}$ are replaced by x in primary loading . Using (20), one can further obtain

$$\frac{\partial \Psi_0^{\boldsymbol{d}}}{\partial \lambda_M^{\boldsymbol{d}}} = \frac{\partial \Psi_0^{\boldsymbol{d}}}{\partial x} = \mathcal{N}_0 N(t,T) \left[\frac{d\Phi(x)}{dx} \int\limits_{D_n(x)} \psi_c(n,x) \mathcal{P}_0(n)\, dn - \frac{dn_{min}(x)}{dx} \Phi(x)\, \psi_c(n_{min}(x), x) \mathcal{P}_0(n_{min}(x)) \right] \tag{B.6}$$

where $n_{min}(x) = \nu x \bar{R}_0$, $\frac{dn_{min}(x)}{dx} = \nu \bar{R}_0$, and

$$\frac{d\Phi(x)}{dx} = \bar{R}_0 \nu \mathcal{P}(n_{min}(x))\, n_{min}(x) \frac{\Phi(x)}{\int\limits_{D_{n_0}(x)} n\, \mathcal{P}_0(n)\, dn}. \tag{B.7}$$

By substituting (B.7) in (B.6), one can obtain

$$\frac{\partial \Psi_0^{\boldsymbol{d}}}{\partial x} = \mathcal{N}_0 N(t,T) \nu \bar{R}_0 \mathcal{P}(n_{min}(x)) \left[n_{min}(x) \frac{\Phi(x)}{\int\limits_{D_{n_0}(x)} n\, \mathcal{P}_0(n)\, dn} \int\limits_{D_{n_0}(x)} \psi_c(n,x) \mathcal{P}_0(n)\, dn - \Phi(x)\, \psi_c(n_{min}(x), x) \right] \leq 0 \tag{B.8}$$

As $N(t,T)\nu \bar{R}_0 \mathcal{P}_0(n_{min}(x))$, and $\Phi(x) > 0$, (B.8) holds if only we have the following inequality

$$\frac{n_{min}(x)}{\int\limits_{D_{n_0}(x)} n\, \mathcal{P}_0(n)\, dn} \int\limits_{D_{n_0}(x)} \psi_c(n,x) \mathcal{P}_0(n)\, dn - \psi_c(n_{min}(x), x) \leq 0 \tag{B.9}$$

(B.9) can be rewritten as

$$n_{min}(x) \int\limits_{D_{n_0}(x)} \psi_c(n,x) \mathcal{P}_0(n)\, dn - \psi_c(n_{min}(x), x) \int\limits_{D_{n_0}(x)} n\, \mathcal{P}_0(n)\, dn \leq 0 \tag{B.10}$$

As $n_{min}(x)$ and $\psi_c(n_{min}(x), x)$ are not functions of n, they can be moved inside the integration, thus

$$\int\limits_{D_{n_0}(x)} \mathcal{P}_0(n) \left[n_{min}(x)\, \psi_c(n,x) - n \psi_c(n_{min}(x), x) \right] dn \leq 0 \tag{B.11}$$

As $n_{min}(x) \leq n$ and the strain energy of the shortest chain is always higher than the energy of the rest of the chains ($\psi_c(n,x) \ll \psi_c(n_{min}(x), x)$), one can conclude $n_{min}(x)\, \psi_c(n,x) - \psi_c(n_{min}(x), x) n \leq 0$ for all $n \in D_{n_0}(x)$. While the bracket in the inequality (B.11) is less than zero for all chain lengths (n), the $\frac{\partial \Psi_0^{\boldsymbol{d}}}{\partial \lambda_M^{\boldsymbol{d}}}$ is always less than zero . Checking

$\frac{\boldsymbol{d}}{\partial \Psi_m} \leq 0$ is pretty similar to what we have done for the $\frac{\boldsymbol{d}}{\partial \Psi_0}$ and for the sake of brevity will not be presented here. While each terms in the inequality (B.5) is less than zero , the proposed model holds the condition of the thermodynamic consistency.

References

[1] S. Kashi, R. Varley, M. De Souza, S. Al-Assafi, A. Di Pietro, C. de Lavigne, and B. Fox, "Mechanical, thermal, and morphological behavior of silicone rubber during accelerated aging," *Polymer-Plastics Technology and Engineering*, 2018.

[2] M. Johlitz, "On the representation of ageing phenomena," *The Journal of Adhesion*, vol. 88, no. 7, pp. 620–648, 2012.

[3] T. Chang, X. Zhang, and H.-L. Cui, "Evolution of terahertz dielectric permittivity of rubber during thermo-oxidative aging," *Microwave and Optical Technology Letters*, vol. 60, 12 2017.

[4] M. Johlitz, N. Diercks, and A. Lion, "Thermo-oxidative ageing of elastomers: A modelling approach based on a finite strain theory," *International Journal of Plasticity*, vol. 63, pp. 138–151, 2014.

[5] C. Yu, G. Kang, and K. Chen, "A hygro-thermo-mechanical coupled cyclic constitutive model for polymers with considering glass transition," *International Journal of Plasticity*, vol. 89, pp. 29–65, 2017.

[6] A. C. Vieira, R. M. Guedes, and V. Tita, "Damage-induced hydrolyses modelling of biodegradable polymers for tendons and ligaments repair," *Journal of biomechanics*, vol. 48, no. 12, pp. 3478–3485, 2015.

[7] A. Bahrololoumi and R. Dargazany, "Hydrolytic aging in rubber-like materials: a micro-mechanical approach to modeling," in *American Society of Mechanical Engineers (ASME) 2019 International Mechanical Engineering Congress and Exposition*, 2019.

[8] M. Lugo, J. E. Fountain, J. M. Hughes, J.-L. Bouvard, and M. F. Horstemeyer, "Microstructure-based fatigue modeling of an acrylonitrile butadiene styrene (abs) copolymer," *Journal of Applied Polymer Science*, vol. 131, no. 20, 2014.

[9] A. Launay, Y. Marco, M. Maitournam, I. Raoult, and F. Szmytka, "Cyclic behavior of short glass fiber reinforced polyamide for fatigue life prediction of automotive components," *Procedia Engineering*, vol. 2, no. 1, pp. 901–910, 2010.

[10] A. K. Shojaei and P. Volgers, "Fatigue damage assessment of unfilled polymers including self-heating effects," *International Journal of Fatigue*, vol. 100, pp. 367–376, 2017.

[11] P. A. Schweitzer *et al.*, *Fundamentals of corrosion: mechanisms, causes, and preventative methods*. CRC press, 2009.

[12] J. Kruželák, I. Hudec, and R. Dosoudil, "Influence of thermo-oxidative and ozone ageing on the properties of elastomeric magnetic composites," *Polymer degradation and stability*, vol. 97, no. 6, pp. 921–928, 2012.

[13] W. Possart and M. Brede, *Adhesive Joints: Ageing and Durability of Epoxies and Polyurethanes*. John Wiley & Sons, 2019.

[14] M. Sinha, A. Izadi, R. Anthony, and S. Roccabianca, "A novel approach to finding mechanical properties of nanocrystal layers," *Nanoscale*, vol. 11, no. 15, pp. 7520–7526, 2019.

[15] K. Loeffel and L. Anand, "A chemo-thermo-mechanically coupled theory for elastic–viscoplastic deformation, diffusion, and volumetric swelling due to a chemical reaction," *International Journal of Plasticity*, vol. 27, no. 9, pp. 1409–1431, 2011.

[16] M. Gigliotti and J.-C. Grandidier, "Chemo-mechanics couplings in polymer matrix materials exposed to thermo-oxidative environments," *Comptes Rendus Mécanique*, vol. 338, no. 3, pp. 164–175, 2010.

[17] M. Gigliotti, J.-C. Grandidier, and M. C. Lafarie-Frenot, "Assessment of chemo-mechanical couplings in polymer matrix materials exposed to thermo-oxidative environments at high temperatures and under tensile loadings," *Mechanics of Materials*, vol. 43, no. 8, pp. 431–443, 2011.

[18] M. Johlitz and A. Lion, "Chemo-thermomechanical ageing of elastomers based on multiphase continuum mechanics," *Continuum Mechanics and Thermodynamics*, vol. 25, no. 5, pp. 605–624, 2013.

[19] A. Lion and P. Höfer, "On the phenomenological representation of curing phenomena in continuum mechanics," *Archives of Mechanics*, vol. 59, no. 1, pp. 59–89, 2007.

[20] K. Kannan and K. Rajagopal, "A thermodynamical framework for chemically reacting systems," *Zeitschrift für angewandte Mathematik und Physik*, vol. 62, no. 2, pp. 331–363, 2011.

[21] H. Mohammadi and R. Dargazany, "A micro-mechanical approach to model thermal induced aging in elastomers," *International Journal of Plasticity*, vol. 118, pp. 1–16, 2019.

[22] H. Mohammadi, A. Bahrololoumi, Y. Chen, and R. Dargazany, "A micro-mechanical model for constitutive behavior of elastomers during thermo-oxidative aging," in *Constitutive Models for Rubber XI: Proceedings of the 11th European Conference on Constitutive Models for Rubber (ECCMR 2019), June 25-27, 2019, Nantes, France*, p. 542, CRC Press, 2019.

[23] H. Mohammadi and R. Dargazany, "Micro-mechanical model for thermo-oxidative aging of elastomers," in *ASME 2018 International Mechanical Engineering Congress and Exposition*, pp. V009T12A028–V009T12A028, American Society of Mechanical Engineers, 2018.

[24] P. Saxena, M. Hossain, and P. Steinmann, "A theory of finite deformation magneto-viscoelasticity," *International Journal of Solids and Structures*, vol. 50, no. 24, pp. 3886–3897, 2013.

[25] J. Zhou, L. Jiang, and R. E. Khayat, "A micro–macro constitutive model for finite-deformation viscoelasticity of elastomers with nonlinear viscosity," *Journal of the Mechanics and Physics of Solids*, vol. 110, pp. 137–154, 2018.

[26] G. Potirniche, A. Pascu, N. Shoemaker, P. Wang, M. Horstemeyer, D. Stillman, and T.-L. Lin, "A visco-hyperelastic model for the thermo-mechanical behavior of polymer fibers," *International Journal of Damage Mechanics*, vol. 20, no. 7, pp. 1002–1020, 2011.

[27] H. Khajehsaeid, M. Baghani, and R. Naghdabadi, "Finite strain numerical analysis of elastomeric bushings under multi-axial loadings: a compressible visco-hyperelastic approach," *International Journal of Mechanics and Materials in Design*, vol. 9, no. 4, pp. 385–399, 2013.

[28] A. Maurel-Pantel, E. Baquet, J. Bikard, J.-L. Bouvard, and N. Billon, "A thermo-mechanical large deformation constitutive model for polymers based on material network description: Application to a semi-crystalline polyamide 66," *International Journal of Plasticity*, vol. 67, pp. 102–126, 2015.

[29] B. Farrokh and A. S. Khan, "A strain rate dependent yield criterion for isotropic polymers: low to high rates of loading," *European Journal of Mechanics-A/Solids*, vol. 29, no. 2, pp. 274–282, 2010.
[30] G. Ayoub, F. Zaïri, M. Naït-Abdelaziz, J. M. Gloaguen, and G. Kridli, "A visco-hyperelastic damage model for cyclic stress-softening, hysteresis and permanent set in rubber using the network alteration theory," *International Journal of Plasticity*, vol. 54, pp. 19–33, 2014.
[31] A. S. Khan, O. Lopez-Pamies, and R. Kazmi, "Thermo-mechanical large deformation response and constitutive modeling of viscoelastic polymers over a wide range of strain rates and temperatures," *International Journal of Plasticity*, vol. 22, no. 4, pp. 581–601, 2006.
[32] J. Pan, *Modelling degradation of bioresorbable polymeric medical devices*. Elsevier, 2014.
[33] Y. Yu, Z. Chang, Y. Qi, and D. Feng, "Research on new technology for offshore heavy oil thermal recovery with rod pumping," *Journal of Petroleum Exploration and Production Technology*, vol. 8, no. 3, pp. 947–955, 2018.
[34] L. Kari, "Dynamic stiffness of chemically and physically ageing rubber vibration isolators in the audible frequency range," *Continuum Mechanics and Thermodynamics*, vol. 29, no. 5, pp. 1027–1046, 2017.
[35] A. C. Vieira, R. M. Guedes, and V. Tita, "Constitutive modeling of biodegradable polymers: Hydrolytic degradation and time-dependent behavior," *International Journal of Solids and Structures*, vol. 51, no. 5, pp. 1164–1174, 2014.
[36] Q. Breche, G. Chagnon, G. Machado, B. Nottelet, X. Garric, E. Girard, and D. Favier, "A non-linear viscoelastic model to describe the mechanical behavior's evolution of biodegradable polymers during hydrolytic degradation," *Polymer degradation and stability*, vol. 131, pp. 145–156, 2016.
[37] T. Pretsch, I. Jakob, and W. Müller, "Hydrolytic degradation and functional stability of a segmented shape memory poly (ester urethane)," *Polymer Degradation and Stability*, vol. 94, no. 1, pp. 61–73, 2009.
[38] C. Slater, C. Davis, and M. Strangwood, "Compression set of thermoplastic polyurethane under different thermal–mechanical-moisture conditions," *Polymer degradation and stability*, vol. 96, no. 12, pp. 2139–2144, 2011.
[39] D. Farrar and R. Gillson, "Hydrolytic degradation of polyglyconate b: the relationship between degradation time, strength and molecular weight," *Biomaterials*, vol. 23, no. 18, pp. 3905–3912, 2002.
[40] E. Richaud, P. Gilormini, M. Coquillat, and J. Verdu, "Crosslink density changes during the hydrolysis of tridimensional polyesters," *Macromolecular Theory and Simulations*, vol. 23, no. 5, pp. 320–330, 2014.
[41] A. Tobolsky, I. Prettyman, and J. Dillon, "Stress relaxation of natural and synthetic rubber stocks," *Journal of Applied Physics*, vol. 15, no. 4, pp. 380–395, 1944. cited By 87.
[42] S. Cantournet, R. Desmorat, and J. Besson, "Mullins effect and cyclic stress softening of filled elastomers by internal sliding and friction thermodynamics model," *International Journal of Solids and Structures*, vol. 46, no. 11-12, pp. 2255–2264, 2009.
[43] A. Andriyana, M. S. Loo, G. Chagnon, E. Verron, and S. Y. Ch'ng, "Modeling the mullins effect in elastomers swollen by palm biodiesel," *International Journal of Engineering Science*, vol. 95, pp. 1–22, 2015.
[44] R. Ogden and D. Roxburgh, "A pseudo–elastic model for the mullins effect in filled rubber," *Proceedings of the Royal Society of London. Series A: Mathematical, Physical and Engineering Sciences*, vol. 455, no. 1988, pp. 2861–2877, 1999.
[45] J. Diani, B. Fayolle, and P. Gilormini, "A review on the mullins effect," *European Polymer Journal*, vol. 45, no. 3, pp. 601–612, 2009.
[46] M. Deroiné, A. Le Duigou, Y.-M. Corre, P.-Y. Le Gac, P. Davies, G. César, and S. Bruzaud, "Accelerated ageing of polylactide in aqueous environments: comparative study between distilled water and seawater," *Polymer degradation and stability*, vol. 108, pp. 319–329, 2014.
[47] H. Tsuji and Y. Ikada, "Properties and morphology of poly (l-lactide) 4. effects of structural parameters on long-term hydrolysis of poly (l-lactide) in phosphate-buffered solution," *Polymer Degradation and Stability*, vol. 67, no. 1, pp. 179–189, 2000.
[48] H. Tsuji and Y. Ikada, "Properties and morphology of poly (l-lactide). ii. hydrolysis in alkaline solution," *Journal of Polymer Science Part A: Polymer Chemistry*, vol. 36, no. 1, pp. 59–66, 1998.
[49] J. S. K. Lim, C. L. Gan, and X. M. Hu, "Unraveling the mechanistic origins of epoxy degradation in acids," *ACS Omega*, vol. 4, no. 6, pp. 10799–10808, 2019.
[50] S. Li, "Hydrolytic degradation characteristics of aliphatic polyesters derived from lactic and glycolic acids," *Journal of Biomedical Materials Research: An Official Journal of The Society for Biomaterials, The Japanese Society for Biomaterials, and The Australian Society for Biomaterials*, vol. 48, no. 3, pp. 342–353, 1999.
[51] S. Harogoppad and T. Aminabhavi, "Diffusion and sorption of organic liquids through polymer membranes. ii. neoprene, sbr, epdm, nbr, and natural rubber versus n-alkanes," *Journal of applied polymer science*, vol. 42, no. 8, pp. 2329–2336, 1991.
[52] S. Li, "Hydrolytic degradation characteristics of aliphatic polyesters derived from lactic and glycolic acids," *Journal of Biomedical Materials Research: An Official Journal of The Society for Biomaterials, The Japanese Society for Biomaterials, and The Australian Society for Biomaterials*, vol. 48, no. 3, pp. 342–353, 1999.
[53] A. Gopferich and R. Langer, "Modeling of polymer erosion," *Macromolecules*, vol. 26, no. 16, pp. 4105–4112, 1993.
[54] M. Wang, X. Xu, J. Ji, Y. Yang, J. Shen, and M. Ye, "The hygrothermal aging process and mechanism of the novolac epoxy resin," *Composites Part B: Engineering*, vol. 107, pp. 1–8, 2016.
[55] R. Long, H. J. Qi, and M. L. Dunn, "Modeling the mechanics of covalently adaptable polymer networks with temperature-dependent bond exchange reactions," *Soft Matter*, vol. 9, no. 15, pp. 4083–4096, 2013.
[56] L. Treloar, *The Physics of Rubber Elasticity*. Oxford University Press, 2005.
[57] C. Miehe, S. Göktepe, and F. Lulei, "A micro-macro approach to rubber-like materials - part i: the non-affine micro-sphere model of rubber elasticity," *Journal of the Mechanics and Physics of Solids.*, vol. 52, p. 2617, 2004.
[58] R. Rastak and C. Linder, "A non-affine micro-macro approach to strain-crystallizing rubber-like materials," *Journal of the Mechanics and Physics of Solids*, vol. 111, pp. 67–99, 2018.
[59] H. Dal, C. Zopf, and M. Kaliske, "Micro-sphere based viscoplastic constitutive model for uncured green rubber," *International Journal of Solids and Structures*, vol. 132, pp. 201–217, 2018.
[60] R. Dargazany and M. Itskov, "Constitutive modeling of the mullins effect and cyclic stress softening in filled elastomers," *Physical Review E*, vol. 88, no. 1, p. 012602, 2013.
[61] A. Ehret, M. Itskov, and H. Schmid, "Numerical integration on the sphere and its effect on the material symmetry of constitutive equations-Â a comparative study," *International Journal for Numerical Methods in Engineering*, vol. 81, p. 189, 2010.

[62] E. Verron, "Questioning numerical integration methods for microsphere (and microplane) constitutive equations," *Mechanics of Materials*, vol. 89, pp. 216–228, 2015.
[63] V. Morovati and R. Dargazany, "Micro-mechanical modeling of the stress softening in double-network hydrogels," *International Journal of Solids and Structures*, vol. 164, pp. 1–11, 2019.
[64] V. Morovati and R. Dargazany, "Improved non-gaussian statistical theory of polymer physicsfor short chains," *Physical Review E*, 2019.
[65] V. Morovati, H. Mohammadi, and R. Dargazany, "A generalized approach to improve approximation of inverse langevin function," in *ASME 2018 International Mechanical Engineering Congress and Exposition*, pp. V009T12A029–V009T12A029, American Society of Mechanical Engineers, 2018.
[66] V. Morovati, H. Mohammadi, and R. Dargazany, "A generalized approach to generate optimized approximations of the inverse langevin function," *Mathematics and Mechanics of Solids*, vol. 24, no. 7, pp. 2047–2059, 2019.
[67] R. Dargazany and M. Itskov, "A network evolution model for the anisotropic Mullins effect in carbon black filled rubbers," *International Journal of Solids and Structures*, vol. 46, p. 2967, 2009.
[68] R. Dargazany and M. Itskov, "Constitutive modeling of the mullins effect and cyclic stress softening in filled elastomers," *Physical Review E*, vol. 88, no. 1, p. 012602, 2013.
[69] V. Morovati and R. Dargazany, "Net v1. 0: A framework to simulate permanent damage in elastomers under quasi-static deformations," *SoftwareX*, vol. 10, p. 100229, 2019.
[70] S. Govindjee, "An evaluation of strain amplification concepts via monte carlo simulations of an ideal composite.," *Rubber Chemistry and Technology*, vol. 70, p. 25, 1997.
[71] J. Bergström and M. Boyce, "Mechanical behavior of particle filled elastomers," *Rubber Chem. Technol.*, vol. 72, p. 633, 1999.
[72] R. Dargazany, V. N. Khiêm, U. Navrath, and M. Itskov, "Network evolution model of anisotropic stress softening in filled rubber-like materials; parameter identification and finite element implementation," *Journal of Mechanics of Materials and Structures*, vol. 7, no. 8, p. 861, 2013.
[73] P.-Y. Le Gac, P. Davies, and D. Choqueuse, "Evaluation of long term behaviour of polymers for offshore oil and gas applications," *Oil & Gas Science and Technology Revue d'IFP Energies nouvelles*, vol. 70, no. 2, pp. 279–289, 2015.
[74] A. Stevenson, "On the durability of rubber/metal bonds in seawater," *International Journal of Adhesion and adhesives*, vol. 5, no. 2, pp. 81–91, 1985.
[75] G. Machado, G. Chagnon, and D. Favier, "Analysis of the isotropic models of the mullins effect based on filled silicone rubber experimental results," *Mechanics of Materials*, vol. 42, no. 9, pp. 841–851, 2010.
[76] A. S. Khan and S. Huang, *Continuum theory of plasticity*. John Wiley & Sons, 1995.